Original Article

Ventricular Tachycardia and Early Fibrillation in Patients With Brugada Syndrome and Ischemic Cardiomyopathy Show Predictable Frequency-Phase Properties on the Precordial ECG Consistent With the Respective Arrhythmogenic Substrate

David Calvo, MD, PhD; Felipe Atienza, MD, PhD; Javier Saiz, PhD; Laura Martínez, BS; Pablo Ávila, MD; José Rubín, MD, PhD; Benito Herreros, MD; Ángel Arenal, MD, PhD; Javier García-Fernández, MD, PhD; Ana Ferrer, MD; Rafael Sebastián, PhD; Pablo Martínez-Camblor, PhD; José Jalife, MD; Omer Berenfeld, PhD

Background— Ventricular fibrillation (VF) has been proposed to be maintained by localized high-frequency sources. We tested whether spectral-phase analysis of the precordial ECG enabled identification of periodic activation patterns generated by such sources.

Methods and Results—Precordial ECGs were recorded from 15 ischemic cardiomyopathy and 15 Brugada syndrome (type 1 ECG) patients during induced VF and analyzed in the frequency-phase domain. Despite temporal variability, induced VF episodes lasting 19.6±7.9 s displayed distinctly high power at a common frequency (shared frequency, 5.7±1.1 Hz) in all leads about half of the time. In patients with Brugada syndrome, phase analysis of shared frequency showed a V_1–V_6 sequence as would be expected from patients displaying a type 1 ECG pattern ($P<0.001$). Hilbert-based phases confirmed that the most stable sequence over the whole VF duration was V_1–V_6. Analysis of shared frequency in ischemic cardiomyopathy patients with anteroseptal (n=4), apical (n=3), and inferolateral (n=4) myocardial infarction displayed a sequence starting at V_1–V_2, V_3–V_4, and V_5–V_6, respectively, consistent with an activation origin at the scar location ($P=0.005$). Sequences correlated with the Hilbert-based phase analysis ($P<0.001$). Posterior infarction (n=4) displayed no specific sequence. On paired comparison, phase sequences during monomorphic ventricular tachycardia correlated moderately with VF ($P<0.001$). Moreover, there was a dominant frequency gradient from precordial leads facing the scar region to the contralateral leads (5.8±0.8 versus 5.4±1.1 Hz; $P=0.004$).

Conclusions—Noninvasive analysis of ventricular tachycardia and early VF in patients with Brugada syndrome and ischemic cardiomyopathy shows a predictable sequence in the frequency-phase domain, consistent with anatomic location of the arrhythmogenic substrate. (***Circ Arrhythm Electrophysiol.*** 2015;8:1133-1143. DOI: 10.1161/CIRCEP.114.002717.)

Key Words: Brugada syndrome ■ electrocardiography ■ myocardial infarction ■ tachycardia, ventricular ■ ventricular fibrillation

On a single-lead ECG, the activation of the ventricles during ventricular fibrillation (VF) appears to be highly complex and continuously changing, conjuring up the idea that VF results from random electric excitation. However, studies in animals[1] and computational models[2,3] in which electric wave propagation has been studied at high resolution have demonstrated that the characteristics of VF in the structurally normal heart are both deterministic and quantifiable, and that they depend on the activation rate of highly periodic reentrant sources that result in fibrillatory conduction with spatial gradients of local activation frequency. Correspondingly, studies in humans using a relatively small number of body surface

<div style="border:1px solid;">

WHAT IS KNOWN

- The mechanisms of ventricular fibrillation in patients with and without structural abnormalities of the ventricles are poorly understood.
- Phase and Frequency analyses of fibrillatory signals have elucidated arrhythmia mechanisms.

WHAT THE STUDY ADDS

- During human ventricular fibrillation the spatial location of the arrhythmogenic substrate implies a hierarchical organization in the phase and frequency domain of electric activity recorded from the body surface that is not consistent with random cardiac activation.
- The method and findings in this study pave the way to deriving further mechanistic insights from noninvasive ECG recordings of ventricular fibrillation and tachycardia, with the potential to improve therapy.

</div>

electrode recordings demonstrated spatiotemporal organization during VF.[4,5] However, it is still unclear whether highly periodic sources also maintain VF in humans and how they relate to the substrate in individual patients with distinct pathology.

As a first approximation, patients with Brugada syndrome (BrS) and ischemic cardiomyopathy (IC) may be considered to be 2 extremes of a continuum in which the structure of the ventricles changes from relatively homogeneous (BrS) to highly heterogeneous (IC), ie, whereas in BrS the ventricles are for the most part structurally uniform, in IC they are substantially remodeled, nonuniform, and variably scarred. Here, we study the possible mechanistic link between the ventricular substrate and the ensuing ventricular tachycardia (VT) and early VF in patients using a novel noninvasive analysis based on the standard precordial ECG leads. We tested the hypothesis that early VF in patients with BrS or IC is spatiotemporally organized by high-frequency sources localized stably at the pathophysiological substrate. We demonstrate that, in the human ventricles, the spatial location of the arrhythmogenic substrate yields a hierarchical organization in the phase and frequency domains that is consistent with a deterministic mechanism of fibrillation.

Methods

Detailed Methods are available in the Data Supplement.

Patients

Patients were admitted for electrophysiology study with either BrS type I ECG or IC with healed myocardial infarction (MI; >6 months). The study was approved by the Ethics Committee, and subjects gave informed consent.

Electrophysiology and Recording Protocol

Standard ECG was recorded continuously at a sampling rate of 1 kHz and band-pass filtered at 0.05 to 150 Hz. The electrophysiology strategy varied according to the clinical indication.

Patients With BrS

We induced VF by programmed stimulation through a transvenous catheter electrode at the right ventricular (RV) apex or at the RV outflow tract. We included only those patients in whom the immediately preceding ECG displayed a type I pattern on the right precordial leads.

Patients With IC

Programmed RV apex stimulation was used for VT induction. We placed another catheter in the left ventricle (LV) for endocardial mapping and ablation as follows: 3-dimensional (3D) endocardial reconstructions were created by CARTO (Biosense Webster) mapping system delineating endocardial scar and dense scar tissues as areas displaying bipolar electrogram amplitudes of <1.5 and <0.5 mV, respectively.[6] Ablation followed mapping of induced or spontaneous sustained VT. Sites displaying presystolic electrograms (within 50 ms before the QRS onset) and fulfilling the criteria of concealed entrainment with equally spike-QRS to electrogram-QRS intervals were marked as the tachycardia exit sites. Pacing was performed for validation. For ethical reasons, the patients with IC included in the study were only those in whom sustained VF was unintentionally induced during the procedure.

Processing of Precordial Signals

Signals from precordial leads were exported, processed by a Hanning window and with a nonbiased 1 to 20 Hz band-pass filter. Thereafter, a 4096-point fast Fourier transformation (FFT; resolution 0.24 Hz) was obtained for frequency-phase analysis. Power and phase versus frequency were calculated for sliding episodes with 15-ms leaps. Dominant frequency (DF) was defined as the frequency with highest power in the spectrum. Shared frequency (SF) was defined as the frequency with power peak lasting >0.5 s simultaneously in all leads (Figure 1). The instantaneous phase was calculated by 2 methods: (1) the ratio of the imaginary to the real components of the FFT at the SF frequency and (2) the Hilbert transform of the entire episode.[7]

Location of the Pathological Substrates, Exit Sites, and Precordial Leads

In patients with BrS, the precordial signals displaying type I morphology marked the location of the functional abnormalities.[8] In a subset of 6 patients with IC, we merged computed tomographic scan images with the CARTO maps for better anatomic reference and marked the positions of the precordial ECG leads on the thorax surface by acquiring the corresponding locations of a roving catheter tip on the CARTO (Figure I in the Data Supplement). We classified dense scars as those being located on the anteroseptal, apical, posterior, or inferolateral LV.

Computer Simulations

We used a realistic 3D computer model of the human heart and torso to simulate body surface potentials during ventricular pacing.

Statistical Analysis

Continuous variables are reported as mean±SD or as 95% confidence interval where noted. In case of a varying number of observations drawn from the subjects, the resampling methods of naive bootstrap[9] and the general bootstrap algorithm[10] were used to make inferences (Data Supplement).

Results

Patients and VF

We studied early sustained VF in 15 patients with BrS and 15 patients with IC (Table). We induced VF in patients with BrS by RV apex (n=14) or RV outflow tract (n=1) pacing. The IC cohort consisted of patients with previous MI of the
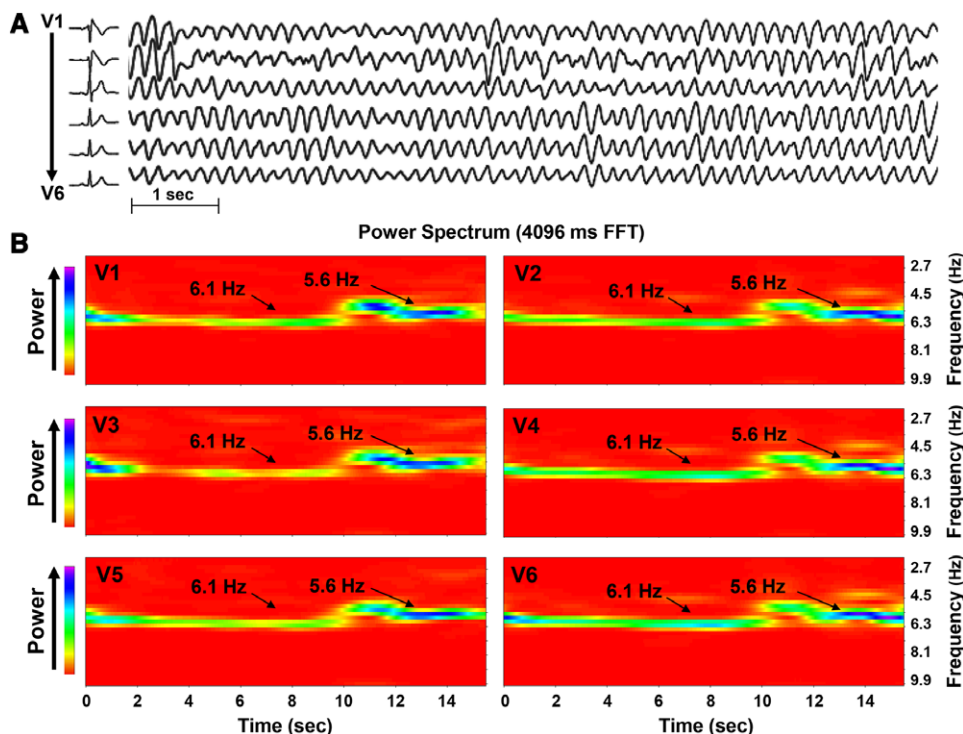
Figure 1. Shared frequency (SF) during ventricular fibrillation (VF) in a patient with Brugada syndrome (BrS). **A**, ECG tracings during SR (**left**, BrS type I at V_1 and V_2) and induced VF (**right**). **B**, Periodograms of 6 precordial signals. Despite temporal variability in **A**, all signals reveal simultaneous and relatively stable power at SF of 6.1 and 5.6 Hz for periods lasting several seconds. FFT indicates Fourier transformation.

anteroseptal (n=4), posterior (n=4), apex (n=3), and inferolateral (n=4) aspects of the LV. The IC patients included those in which VF was unintentionally induced while pacing from the RV apex (n=11), delivering antitachycardia pacing (n=2) or moving the catheters (n=2).

Precordial Frequency-Phase Domain Organization of VF in Patients With BrS and IC

Figure 1 shows sample VF data from a patient with BrS. The tracings in Figure 1A are simultaneous precordial lead recordings during sinus rhythm and induced VF. The sinus rhythm signals show a type I BrS ECG at V_1 and V_2 (left) indicating an abnormal arrhythmogenic substrate at the RV outflow tract.[11] Figure 1B shows the power spectra of sliding periods of signals from V_1–V_6 during VF in the same patient. Despite signal variability in time and between leads, the periodogram of each precordial clearly shows narrow peak power at SFs of 6.1 and 5.6 Hz. Overall, VF episodes recorded for 19.6±7.9 s in the 30 patients with BrS and IC contained 57 long-lasting epochs (3.4±2.1 s; range 0.7–8.7 s) of SFs corresponding to 44.5±24.5% of the time through the whole spectrogram. In the other, 55.5% VF was characterized by power distributed at different frequencies on each precordial lead, possibly reflecting more complex activity when compared with episodes with a SF. Both the duration and the number of SFs were similar in patients with BrS and IC (3.6±1.9 versus 3.3±2.2 s; *P*=0.591 and 1.8±0.8 versus 1.7±0.9 s; *P*=0.667, respectively). The overall SF in all leads was 5.7±1.1 Hz; however, SFs in patients with BrS tended to be higher than patients with IC (6.1±0.7 versus 5.3±1.3 Hz, respectively; *P*=0.065).

We next investigated whether the VF activity recorded in the precordial leads maintained predictable phase sequences. Figure 2A shows the time-course of the phases at the 2 distinctive SFs in the 6 precordials in the same patient with BrS during the VF episode shown in Figure 1A. The phase distribution (black arrow) and propagation (red arrow) between precordials occurred in well-demarcated clusters for the 57 SFs

Table.   Patients Characteristics

	Patients With BrS (n=15)	Patients With IC (n=15)	*P* Value
Age, y	42.9±11.6	66.2±8.5	<0.001
LVEF, %	62.6±2.6	41.8±9.8	<0.001
CHF	0 (0%)	2 (13.3%)	0.483
β-Blockers	0 (0%)	10 (66.7%)	<0.001
Amiodarone	0 (0%)	3 (20%)	0.224
Sotalol	0 (0%)	1 (6.7%)	1.000
Class I	0 (0%)	0 (0%)	*
Substrate location			
Anteroseptal	15 (100%)	4 (26.7%)	…
LV apex	0 (0%)	3 (20%)	…
LV inferolateral	0 (0%)	4 (26.7%)	…
LV posterior	†	4 (26.7%)	…

BrS indicates Brugada syndrome; CHF, congestive heart failure; Class I, class I antiarrhythmic therapy; IC, ischemic cardiomyopathy; and LVEF, left ventricular ejection fraction; and ns, not significant.
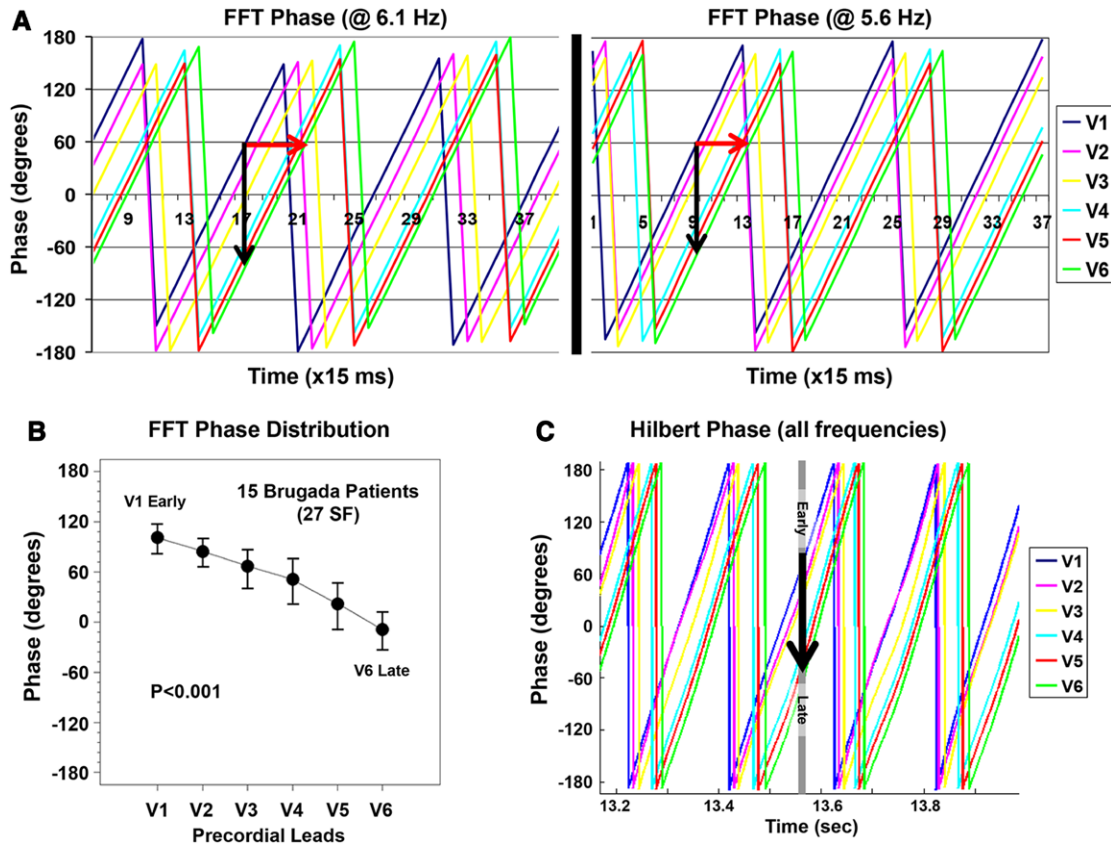
*Not computed.

†No ECG criteria.

Figure 2. Phase's analysis during induced ventricular fibrillation (VF) in Brugada syndrome. **A**, The time course of phases of the sample precordials shown in Figure 1 is characterized by well-demarcated clusters. Black arrow, instantaneous phase distribution across leads; red arrow, phase propagation across leads. **B**, Cumulative fast Fourier transformation (FFT)–based phases at SF demonstrate a consistent sequence from V_1–V_2 (early) to V_5–V_6 (late). Time for phase determination was at phase ≈0 in the middle of the cluster. Error bars: 95% CI. **C**, Hilbert transform provides the time course of phases for all frequencies. The phase distribution of the signals shown in Figure 1 denotes a sequence from early to late (black arrow) similar to the FFT-based phases at specific SF shown in **A**. Time in all panels is measured from initiation of VF.

detected in patients with both BrS (27 SFs) and IC (30 SFs). The width of the clusters in those 57 sequences (measured by the length of the vertical black arrow) was 134.3°±46.2°, which was significantly narrower than a nonclustering distribution ($P<0.001$ versus 180° with similar SD; ie, a range including antiphases). The order of phases in the clusters varied depending on the location of the specific arrhythmogenic substrate responsible for the arrhythmia. All patients with BrS were characterized by a type I ECG pattern with typical ST-segment elevation in V_1 and V_2, which corresponded to an anteroseptal location of the arrhythmogenic substrate. In these patients, the sequence of the phases (either distribution or propagation) was from V_1–V_2 to V_5–V_6 in 21 of the 27 SFs (77.8%), whereas a sequence originating in V_3–V_4 or V_5–V_6 was observed in 2 (7.4%) and 4 (14.8%) SFs, respectively ($P<0.001$). In Figure 2B, cumulative data show that the phases of V1 were of higher degree (early) in the cluster than V_6 (late), with a monotonic decrease from right (V_1) to left (V_6; $P<0.001$) precordials, according to their location in the frontal axis (Figure I in the Data Supplement).

Because the sequence and phase distribution shown in Figure 1B are necessarily time-invariable by virtue of the FFT at a particular frequency (ie, the SF), we investigated the temporal stability of the phases using also the Hilbert transform,

which yields the instantaneous phase of the activity, considering the entire spectral content. Figure 2C shows the Hilbert-based phases of the 6 precordial leads during the same VF episode as in Figure 1. Similar to the FFT-based phases, Hilbert-based phases clustered in well-defined groups. Most importantly, their temporal intrabeat sequence (ie, from V_1 and V_2 [early] to V_5 and V_6 [late]) was remarkably stable, which is in accordance with both the FFT analysis and the stability of the SF in this patient with BrS. Considering all patients with BrS together, the Hilbert-based phase sequences were found to be more frequently originating from V_1 to V_2 than from V_5 to V_6 (88.9% versus 11.1%, respectively; $P<0.001$), showing substantial agreement with the sequence of FFT-based phases (Figure II in the Data Supplement).

Precordial Phase Sequences During VF in Patients With IC

In patients with IC, the phase distribution and propagation of each of the 30 SFs during VF sequenced in relation with the location of the scar tissue in 63.3% ($P=0.038$). Figure 3 shows VF data and phase analysis from an IC patient with a septal MI. As shown in A and B, early VF in that patient was characterized by an SF of ≈5.8 Hz. The time-course of the precordial phases shown in C demonstrates clustered activity
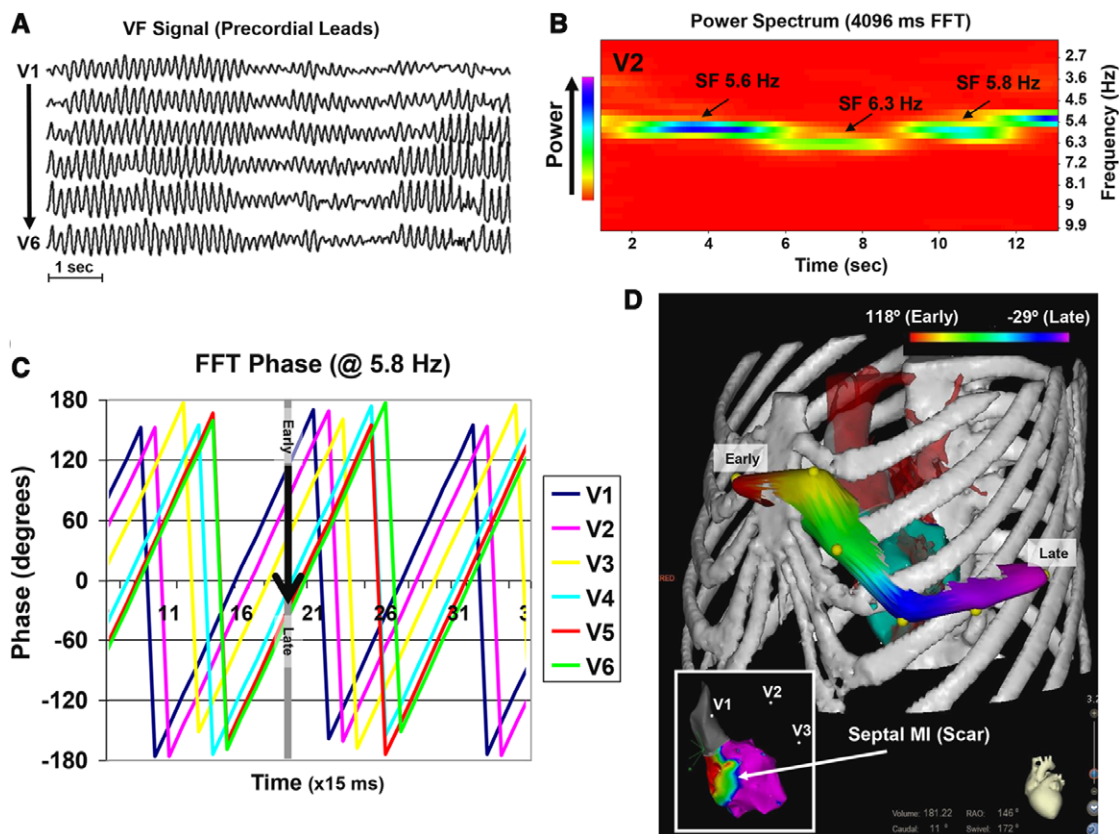
Figure 3. Ischemic cardiomyopathy; phases analysis during ventricular fibrillation (VF) in patient with a septal myocardial infarction (MI). **A**, Precordial signals during VF. **B**, Periodogram of V_2 showing high power around 5.6, 6.3, and 5.8 Hz. **C**, The phase's time course at 5.8 Hz reveals a sequence from V_1 to V_6 (black arrow from early to late). The same alignment was observed for 5.6 and 6.3 Hz. **D**, Phase distribution superimposed on the thorax map illustrates that the sequence from V_1 to V_6 is consistent with activation originating close to the MI scar location (inset, red is <0.5 mV). FFT indicates fast Fourier transformation.

with an intrabeat sequence of V_1 (early) to V_6 (late). In D, the intrabeat phase distribution across the precordials is displayed on the 3D torso map (Figures I–III in the Data Supplement) to confirm that the earliest beat-phase is at V_1 (red), closest to the MI location, and the latest beat-phase is at V_6 (purple). In Figure 4A and 4B, we use CARTO maps to illustrate 2 additional examples of distinct relationships between the scar location and the distribution of precordial phases of SFs during VF in patients with IC. In A, a patient with an inferolateral MI presented a VF episode with SF of 5.8 Hz and a V_6–V_1 intrabeat phase sequence. In B, another patient with an LV apex MI developed VF with SF of 4.8 Hz with the earliest phase at V_3–V_4 and spread toward V_1 and V_6. However, the latter behavior was not representative of all patients with either LV apex or posterior LV MI, as the phase sequence varied substantially from one patient to the next. Figure 4C and 4D shows phase distributions across the precordial leads of patients with anteroseptal and inferolateral scars. Data from 8 SFs in 4 patients with anteroseptal scars showed a monotonic distribution from early V_1 to late V_6 ($P<0.001$; Figure 4C), consistent with the precordials location along the frontal axis. In contrast, Figure 4D shows that in 9 SFs from 4 patients with inferolateral scar the distribution of phases was such that V_6 was earlier than V_1 ($P<0.001$), V_2 ($P<0.001$), and V_3 ($P=0.048$), with V_1 having the lowest phases in the cluster`s alignment ($P<0.001$). The monotonic decrease of phases from

V_6 to V_1 was not statistically significant when considering all precordials ($P=0.245$), probably because of large variability at V_4. Yet the differences between lateral (V_6) and right (V_1, V_2, and V_3) precordial leads demonstrate that the distribution of phases reverses in patients with inferolateral scars relative to those with anteroseptal scars (see also below).

VF Phase Sequence and Wave Origin in Patients With IC

Figure 5A shows the location of the precordials (Figures I and III in the Data Supplement) relative to the heart to provide a geometric reference of the VF phase distribution across leads. In B, we show the FFT-based time-space plot of phases of SF in 3 sample VF cases with 3 different MI locations. The color-coded phases (white arrows) are seen to propagate across leads (black arrows) in distinct sequences, consistent with what is shown in Figures 3 and 4: for anteroseptal and inferolateral MIs, the phases propagate from V_1 to V_6 and V_6 to V_1, respectively, whereas for a LV apex MI, the phases spread from V_4 to V_1 and V_6.

To further validate the correlation between the precordial sequences and the ventricular origin of waves, we used a computer model of the ventricles inside the torso to simulate paced activity and calculate the phase distribution on the precordial body surface locations. In Figure IV in the Data Supplement, pacing the septum, the LV apex, and the lateral LV yielded
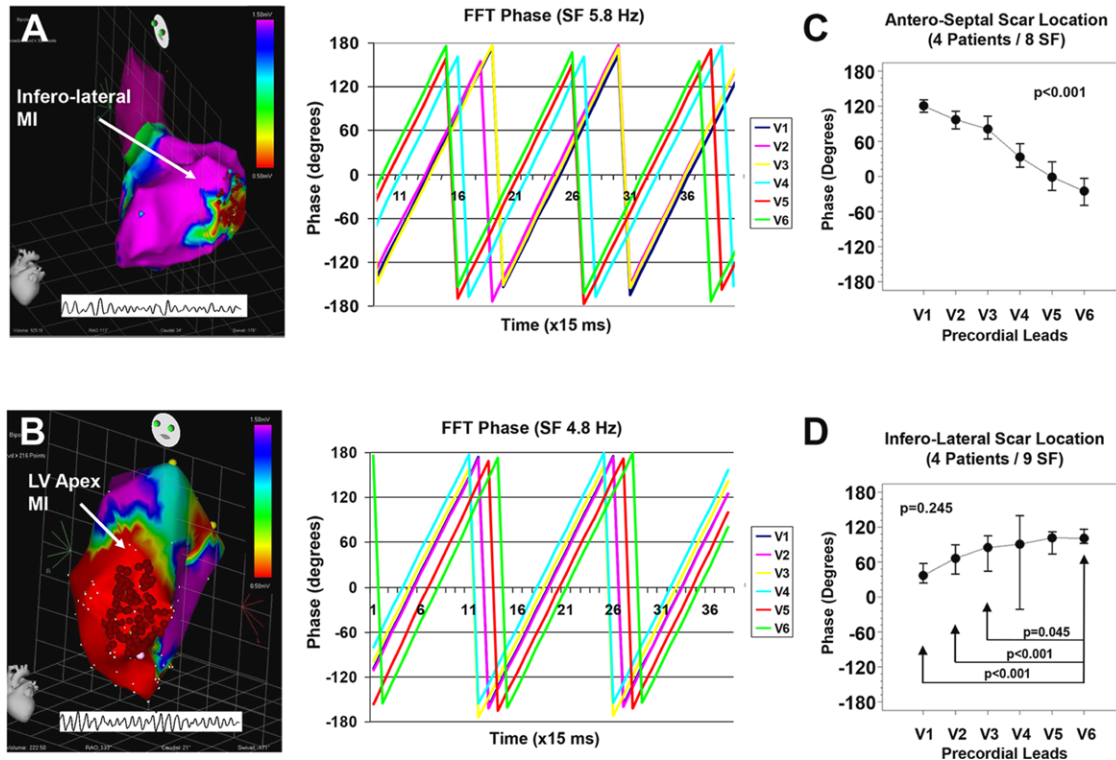
Figure 4. Ischemic cardiomyopathy; phases during ventricular fibrillation (VF) and localized myocardial infarctions (MIs). **A**, Electroanatomic map showing an left ventricular (LV) inferolateral myocardial infarction (MI), sample VF recording and corresponding VF phases time course at shared frequency (SF) = 5.8 Hz. The earliest lead is V_6. **B**, Electroanatomic map showing an LV apex MI, sample VF recording, and corresponding VF phases time course at SF = 4.8 Hz. The earliest lead is V_4. **C**, Patients with anteroseptal scar display a steady sequence of propagation from V_1 to V_6. **D**, In contrast, inferolateral scar patients display a sequence from V_6 to V_1. Error bars, 95% CI.

similar sequences of phase propagation in the precordial leads as in Figure 5B, confirming our interpretation that the patterns of sequences depended on the directionality of ventricular wave propagation during VF.

To determine how precordial phase propagation patterns were affected by the scars exit sites, we performed simulations in which we paced at opposite sides of conduction block lines representing scars similar to those of patients with IC in Figures 3 and 4. Figure VA in the Data Supplement shows that contralateral exit sites from scars that span 30% to 40% of the long axis of the LV and are located on the anteroseptal and inferolateral LV walls produce waves that move transiently in opposite directions, but subsequently follow propagation patterns that are similar for each block line, irrespective of the initial propagation direction. In Figure VB in the Data Supplement, phase propagation graphs are somewhat sensitive to the initial directionality of the exiting wave, but the sequence of the phases is mainly determined by the spatial location of the pacing site; ie, V_6 and V_5 precede other precodials when pacing the lateral wall; V_1 and V_2 precede other precordials when pacing the septum. Thus, the sequence of precordial phases in the patients with IC analyzed in Figures 3 and 4 depends more on the scar location than on the precise exit site from that scar.

Because VF may contain frequency components other than SFs, each with its own phase sequence, we calculated the Hilbert-based phases of the precordial leads recorded during VF and compared their sequence with the FFT-based phase at the SFs contributing to the same ECGs. Figure 5C demonstrates

that when all the frequency components of the 3 sample VF signals with similar MI location as in Figure 5B are considered, the propagation of phases remains generally similar to when only a single SF is considered. Further comparison of the leads at which the phases originated in the FFT-based phase analysis with those in the Hilbert-base analysis revealed a highly significant concordance (к̂ concordance coefficient 0.741 [95% confidence interval, 0.497–0.938]), mainly when the origin was at V_1–V_2 or V_5-V_6 (Figure II in the Data Supplement). Overall, patients with anteroseptal, apical, and inferolateral LV MIs tend to display a steady sequence of phases originating at V_1–V_2, V_3–V_4, or V_5–V_6, respectively (Figures 3 and 4). Also, as shown in Figure VI in the Data Supplement, pacing from 2 different areas in the RV (outflow tract and apex; 5 patients) displayed different phase propagation patterns depending on the location of the stimuli and the direction of electric propagation.

Correlation Among Phase Sequences in VT and VF

We further tested the hypothesis that the arrhythmogenic substrate in the ventricles determines the activation directionality during both VT and VF. We used paired comparisons between the mapped VTs and sustained VFs in the group of patients who developed both arrhythmias (n=10). As shown in Figure 6, phase propagation in VF was similar to VT in a patient with inferolateral MI. Figure 6A shows a monomorphic VT that subsequently transformed into VF. Despite the complexity of the precordial VF signals in the time domain, the sampled V_1 and V_6 periodograms in B reveal that a peak power
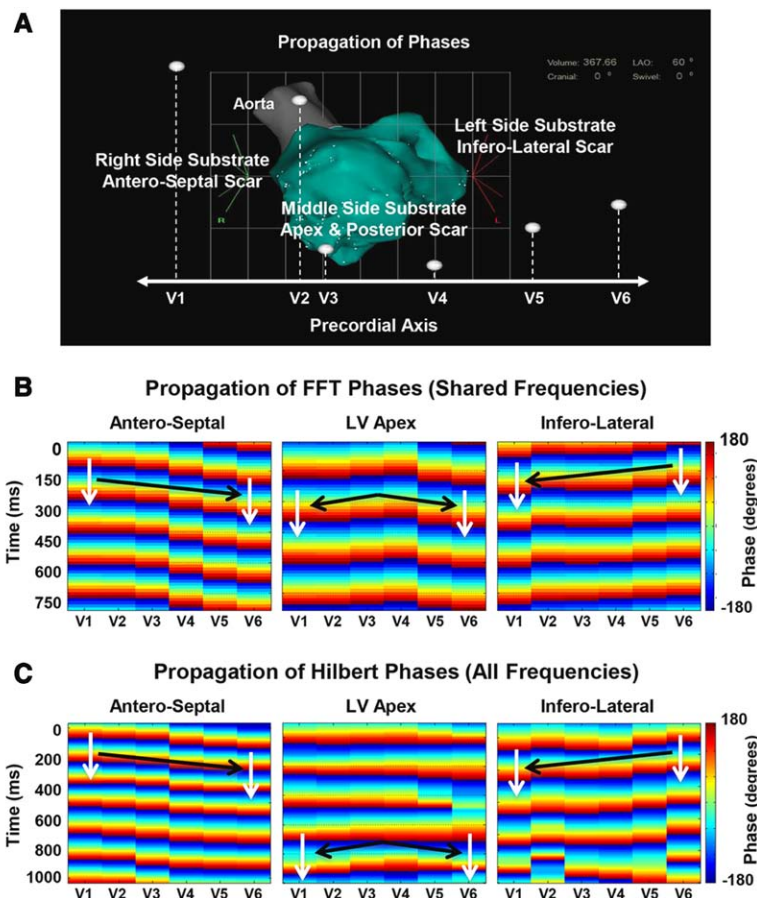
Figure 5. Propagation of precordial phases during ventricular fibrillation (VF). **A**, Precordial leads diagram superimposed on a sample CARTO map of the left ventricular (LV) across the coronal plane. **B**, Dependency of the directionality of fast Fourier transformation (FFT)–based phase propagation on the location of the scar; in 3 sample patients the progression of the phase reverses from V$_1$ to V$_6$ (**left**) to V$_6$ to V$_1$ (**right**) as the location of the scar changes from the anteroseptal to the inferolateral aspects of the LV. **C**, Equal sequences are obtained by Hilbert-based phases that account for all frequency components of each signal.

at SF ≈5.8 Hz is present for a significant portion of the VF episode analyzed. Figure 6C shows the phase analyses during VT (left) and VF (right) in the same patient. The phase propagation sequence across the precordials was similar despite the different SFs that characterized each of the 2 arrhythmias; the sequence was from V$_6$ to V$_1$ in both.

Figure 7 summarizes the relationships among the sequences of the precordial phases during VF and VT. In A, data from 10 patients show that the VT and VF phases at SF of the same leads correlate moderately but significantly (linear correlation coefficient, 0.64; *P*<0.001). The relationship between the VT and VF phases is further quantified in B by a histogram of their differences (δ phase) along with the kernel distribution density estimation: the distribution of δ phase is well concentrated around a mean close to 0 (peak, −6.01; 95% confidence interval, −19.06, 5.57°), with 60% of the phases during VF being ≤30° different from the phases during VT in the same patient (95% confidence interval, 49%–71%). Figure 7C and 7D illustrates the coarse relationship that exists between leads at which the phase originates during VT/VF and the location of the arrhythmogenic scar in patients with IC. The VT graph in C demonstrates that as the arrhythmogenic site shifts from the right (anteroseptal) to the middle (apex) and to the left (inferolateral) of the LV of different patients, a concomitant shift in the earliest VT phase of V$_1$–V$_2$, to V$_3$–V$_4$ and to V$_5$–V$_6$ is observed (*P*<0.001). In D, the relationship between leads with the earliest phase and the site of the substrate during VF is less pronounced than in VT, mainly because the earliest lead

is not uniquely determined for VF with apical and posterior substrate location. Nevertheless, when considering all the analyzed cases together, also during VF the earliest phases at the leads are significantly associated with the substrate location (*P*=0.005). Comparison between C and D leads us to conclude that the phase propagation of high-frequency periodicities during VF is equivalent to the behavior of monomorphic VT phase propagation and its relation with the scar location.

On Hilbert-base phase calculation (Figure II in the Data Supplement) VF was characterized by a similar phase activity on the precordial leads as detected at SFs, which further established that the correlation between the substrate and the precordial phases is independent of the SFs. Finally, to confirm the tight geometric relationship between the sequential distribution of phases on the precordial leads and the arrhythmogenic substrate, we compared their relative position on the body surface and on the heart. Angular analysis presented in Figure VII in the Data Supplement demonstrates a good correlation between the azimuths of the precordial with earliest phase, the arrhythmogenic substrate, and the VT exit sites within a common short-axis plane of the torso.

Hierarchical Precordial DFs Localizes the Arrhythmogenic Area

The SFs across the precordials during VF were not necessarily the DFs in the spectrogram for those leads; however, they were usually the DFs on the leads that were closest to the substrate. Figure 8A shows power spectra of the precordials in an
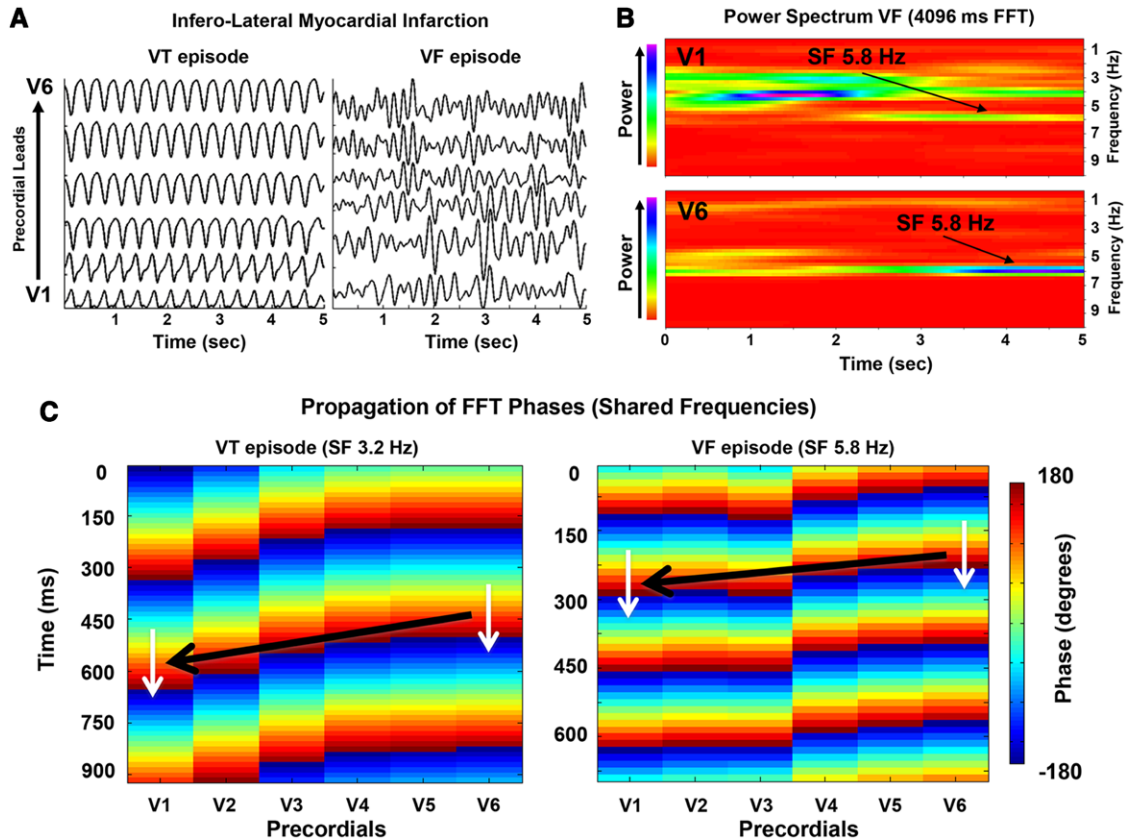
Figure 6. Phase distribution during ventricular tachycardia (VT) and ventricular fibrillation (VF) in an ischemic cardiomyopathy patient. **A**, ECG tracings during VT (**left**, frequency of 3.2 Hz) and VF (**right**) in a patient with an inferolateral scar. **B**, The periodogram during VF shows that 5.8 Hz is the highest frequency to contain significant power for most of the recording time in V_6 and V_1. **C**, Phase propagation sequence is similar for VT at 3.2 Hz and VF (shared frequency) at 5.8 Hz (V_6–V_1).

IC patient with inferior MI. A 5.85 Hz peak is present in the spectra of all leads, but it is the DF only at V_5 and V_6. It is the highest frequency peak among all leads and is located closest to the scar in this patient. To study the relationship between the hierarchy of the DFs and the location of the scar, we compared the DFs in the leads near the scar and those in the contralateral leads. Figure 8B summarizes the DF data in 11 IC patients with VF (patients with posterior scar were excluded). In 6 of 11 patients, a precordial DF gradient was observed between the scar and the contralateral locations. Considering all the patients with IC, with and without a gradient, we found the DF closest to the substrate to be higher than the DF contralateral to the substrate (5.8±0.8 versus 5.4±1.1 Hz; $P=0.004$).

The precordial DF distribution in patients with BrS was found to be more uniform than the IC patients, with only 2 of the 15 patients displaying a DF gradient ($P<0.001$). The SF value at each precordial was the same as the DF value, regardless of whether it was close to the substrate location (SF 6.1±0.7 Hz versus DF 6.1±0.7 Hz; $P=0.327$) or more distally (SF 6.1±0.7 Hz versus DF 6.1±0.7 Hz; $P=0.476$). Obviously, at a mean uniform value of 6.1 Hz, a DF gradient in our BrS cohort is nonexistent ($P=0.648$).

Cardiac Function and VF Dynamics
Interestingly, the cardiac function of patients during sinus rhythm was related to electric dynamics during VF. Considering the precordial DF values during VF, both BrS and IC

patients with no DF gradient had higher LV ejection fraction (60.6±8.9%; n=18) than patients with a DF gradient (44.7±14.7%; $P=0.002$; n=8; Figure 8C). As expected, patients with BrS had no cardiac structural abnormalities as quantified by echocardiogram. In patients with IC, we observed a trend toward significantly higher LV ejection fraction in patients with no DF gradient (49.2±10.6%) than in those with a DF gradient (38±9.1%; $P=0.091$). Lack of statistical significance at $P<0.05$ in the patients with IC is because of low power, possibly related to their generally lower LV ejection fraction than that in the patients with BrS, requiring further study.

Discussion
The main findings of this study are that the signals of the 6 precordial ECG leads during VT and VF in patients with BrS and IC follow a sequence in the phase-domain that is distinctly related to the location the pathophysiologic substrate. Using frequency-phase domain analysis across the standard precordial leads, we demonstrate hierarchical distributions of frequencies and phases suggesting that in many individual patients the arrhythmias are driven from a substrate location, with higher source frequency in VF versus VT. Thus, our results are consistent with a nonrandom mechanism of VF and support the idea that a relatively small number of stable sources maintain VF in both the structurally normal and the diseased human heart.
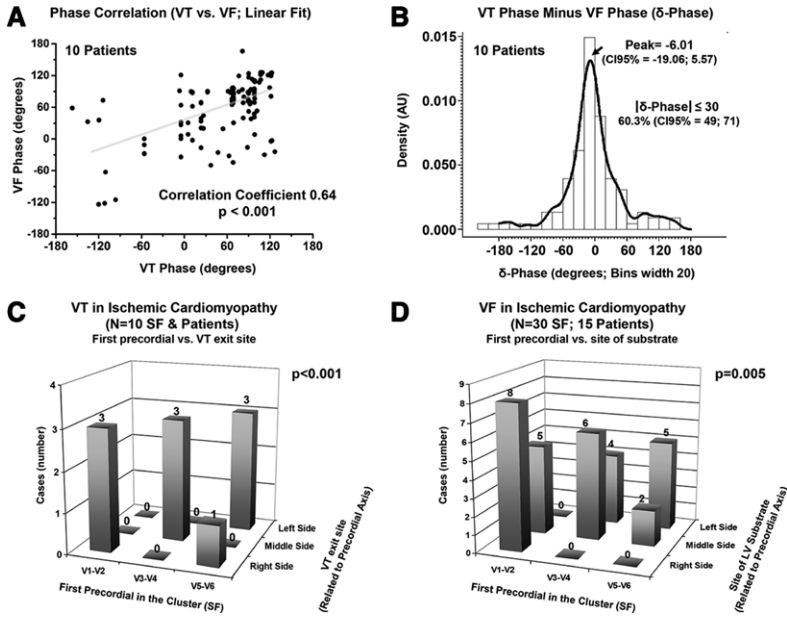
Figure 7. Phase sequences in ventricular fibrillation (VF) and ventricular tachycardia (VT). **A,** Correlation between VT and VF phases in similar leads in 10 patients. Time for determination of phase distribution was selected as the time when the earliest lead was at ≈120°. **B,** Histogram (bin = 20°) of the differences between the VF and the VT phases (δ phase) of data from **A** along with the kernel distribution density estimation (see text). **C,** Origin of VT phase sequence and the exit site or the arrhythmogenic scar in ischemic cardiomyopathy (IC) patients: the phase origin reverses from V_1–V_2 to V_5–V_6 as the exit site of the VT changes from the anteroseptal (**right**) to the inferolateral (**left**) aspects of the left ventricular (LV). **D,** Origin of VF phase sequence in IC patients displayed similar dependency of phase origin on site of LV substrate as in VT in **C**. SF indicates shared frequency.

Deterministic Activation During Fibrillation

Early experimental studies in structurally normal rabbit and guinea-pig hearts demonstrated stable and fast rotors driving VF[1,12] and generating high-frequency waves interacting with the surrounding myocardium giving rise to fibrillatory conduction and irregular ECG.[13,14] In the structurally normal heart of the sheep, fibrillatory conduction is reflected as excitation organized in DF domains connected by Wenckebach-like conduction block patterns at their boundaries.[15] In both animals[16] and humans,[17] the DFs of excitation waves have been found to underlie the frequency domain of specific ECG leads on the thorax. During VF in our patients, there were both surface spectral components in the form of SF across the precordial leads and sequential phase distributions (Figures 6 and 7) that were consistent with patterns of waves arising from a region containing an arrhythmogenic substrate (Figures III and IV in the Data Supplement).

Our findings are consistent with the pioneering work of Clayton et al[4,5] who analyzed VF recordings and found a similar frequency content at 3 ECG orthogonal leads 58% of the
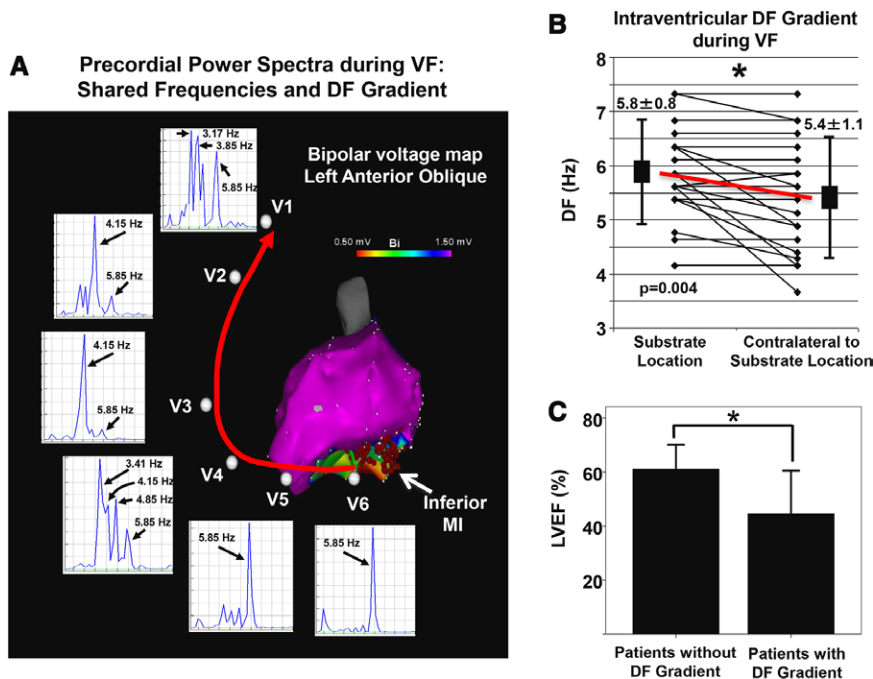

Figure 8. Dominant frequency (DF) gradient at precordials during ventricular fibrillation (VF). **A,** Representative example of DF gradient in a patient with ischemic cardiomyopathy (IC). Power at a shared frequency (SF) of 5.85 Hz is noted. However, this frequency is dominant only at V_6 and V_5 and lower frequencies are dominant in the other precordials; the lowest DF of 3.17 Hz is in V_1. **B,** DF during VF in patients with IC (n=10; 18 SF) shows statistically higher values in precordial leads closest to substrate location. **C,** LV ejection fraction (LVEF) was significantly higher in patients without (n=18) than with (n=8) a DF gradient.

time, with small variability in the phase relationship between leads.

Others have found rotors in the human ventricle under different conditions.[18,19] However, whether these highly periodic sources drive the spatiotemporal organization that we found in our patients or simply coexist as epiphenomena embedded in a multiple-wavelet self-sustained system remains controversial. Recently, Bradley et al[20] studied in vivo human VF and found that the global ischemia produced by the arrhythmia decreased DFs while increasing the number of wavebreaks, the hallmark of rotor formation. Consistent with our study, Nair et al[19] used plunge needles in Langendorff-perfused human hearts and identified 3D rotors during early VF to localize in regions of greater intramural fibrosis.

Regional Ischemia and Organization of VF

Experimental studies have demonstrated that the epicardial border zone of the myocardial scar is prone to sustain reentrant sources of fast VT in animal models.[21] Coromilas et al[22] confirmed that dynamic anisotropy in the periphery of the scar supports short-cycle reentry after action potential shortening by pinacidil. In a pig model of regional ischemia, Zaitsev et al[23] reported that the distribution of wavebreaks during VF is particularly high at the border zone, which exhibits also the largest heterogeneity of excitation frequencies, including highest local DFs. Although no sustained reentry driving VF was registered in those studies, the conjecture was that the wavebreaks in the border zone contributed to the VF by providing a perpetuation mechanism for source formation and maintenance. Overall, the regional scar and ischemia conditions in the experimental studies reflect the importance of particular myocardial areas in facilitating reentry during fibrillation,[24–26] giving credence to the idea that regular firing sources at the periphery of the scar drive VF in our patients.

Local high-frequency periodicity during VF points to a potential driver location similar to that observed during monomorphic VT at a slower frequency.[15] Because mapping and ablation determined that the exit site of the VT was closely related to the scar, we suggest that periodicities observed during VF reflect centrifugal activity from a similar scar region. Previous studies in human hearts demonstrated that fibrosis increased wavebreaks and turbulent propagation, but also stabilized reentry.[19,27] Our data demonstrate that an intraventricular DF gradient exists during early VF in patients with the lowest LV ejection fraction during sinus rhythm (Figure 8). These observations support the notion that VF in our patients originates from high-frequency sources localized to a regional arrhythmogenic substrate and further include widespread, slower fibrillatory activity.

Limitations

All VF episodes were induced and therefore the mechanisms identified may not apply to spontaneous VF. However, similar to the atria, induced VF likely mimics spontaneous VF.[28] Some patients with IC were under β-blocker treatment, which could have converted their VF to be driven by a single source.[29] Nevertheless, the fact that similar sequences of phases were observed during VF in patients with BrS that were devoid of β-blockers suggests that the location of the VF source(s) in all patients was related to the location of their scar. As for the data acquisition, the small number of electrodes and their position on the body surface limit the sensitivity of our analysis for possible complex activation patterns and may bias toward a localized source mechanism of VF. In addition, the nonuniqueness of the relation between epicardial potentials and the myocardial waves limits our interpretation. Indeed, scarcity of intracardiac data precludes exclusion of scenarios in which there is no relationship between origin of VT/VF waves and precordial sequences. However, the match between epicardial and nearest body surface potentials demonstrated by Burnes et al,[30] as well as the fact that both patients and simulations demonstrate a clear relationship between pacing sites and the precordial sequences, diminishes the impact of such limitations. Finally, despite significant positive relationship between phases and scar locations in patients with anteroseptal and inferolateral scars, the configuration of the 6 precordials precluded us from establishing specific phase sequences in patients with either LV apex or posterior LV MI.

Conclusions and Clinical Implications

Ablating substrates to prevent VT[31] and VF[11,32] recurrences in humans is now common. Here, we demonstrate that early VF in patients with BrS and IC is characterized by a reproducible phase sequence in the precordial leads consistent with waves originating from the location of the arrhythmogenic substrate. In addition, we demonstrate that there is a hierarchical precordial lead distribution of DF with values decreasing away from the lead closest to the arrhythmogenic substrate location. Together, the hierarchical distribution of precordial phases and DFs suggests that the mechanism that sustains early VF can be attributed to relatively small number of high-frequency sources that could be targeted more effectively with noninvasive guidance.

References

1. Gray RA, Jalife J, Panfilov AV, Baxter WT, Cabo C, Davidenko JM, Pertsov AM. Mechanisms of cardiac fibrillation. *Science*. 1995;270:1222–1223; author reply 1224.
2. Keldermann RH, ten Tusscher KH, Nash MP, Bradley CP, Hren R, Taggart P, Panfilov AV. A computational study of mother rotor VF in the human ventricles. *Am J Physiol Heart Circ Physiol*. 2009;296:H370–H379. doi: 10.1152/ajpheart.00952.2008.

3. ten Tusscher KH, Mourad A, Nash MP, Clayton RH, Bradley CP, Paterson DJ, Hren R, Hayward M, Panfilov AV, Taggart P. Organization of ventricular fibrillation in the human heart: experiments and models. *Exp Physiol*. 2009;94:553–562. doi: 10.1113/expphysiol.2008.044065.

4. Clayton RH, Murray A, Campbell RW. Evidence for electrical organization during ventricular fibrillation in the human heart. *J Cardiovasc Electrophysiol*. 1995;6:616–624.

5. Clayton RH, Murray A, Campbell RW. Analysis of the body surface ECG measured in independent leads during ventricular fibrillation in humans. *Pacing Clin Electrophysiol*. 1995;18:1876–1881. doi: 10.1111/j.1540-8159.1995.tb03835.x.

6. Arenal A, del Castillo S, Gonzalez-Torrecilla E, Atienza F, Ortiz M, Jimenez J, Puchol A, García J, Almendral J. Tachycardia-related channel in the scar tissue in patients with sustained monomorphic ventricular tachycardias: influence of the voltage scar definition. *Circulation*. 2004;110:2568–2574. doi: 10.1161/01.CIR.0000145544.35565.47.

7. Warren M, Guha PK, Berenfeld O, Zaitsev A, Anumonwo JM, Dhamoon AS, Bagwe S, Taffet SM, Jalife J. Blockade of the inward rectifying potassium current terminates ventricular fibrillation in the guinea pig heart. *J Cardiovasc Electrophysiol*. 2003;14:621–631.

8. Yan GX, Antzelevitch C. Cellular basis for the Brugada syndrome and other mechanisms of arrhythmogenesis associated with ST-segment elevation. *Circulation*. 1999;100:1660–1666. doi: 10.1161/01.CIR.100.15.1660.

9. Efron B, Tibshirani RJ. *An Introduction to the Bootstrap*. New-York: Chapman & Hall; 1993.

10. Martínez-Camblor P, Corral N. A general bootstrap algorithm for hypothesis testing. *J Stat Plan Inference*. 2012;142:589–600. doi: 10.1016/j.jspi.2011.09.003.

11. Nademanee K, Veerakul G, Chandanamattha P, Chaothawee L, Ariyachaipanich A, Jirasirirojanakorn K, Likittanasombat K, Bhuripanyo K, Ngarmukos T. Prevention of ventricular fibrillation episodes in Brugada syndrome by catheter ablation over the anterior right ventricular outflow tract epicardium. *Circulation*. 2011;123:1270–1279. doi: 10.1161/CIRCULATIONAHA.110.972612.

12. Samie FH, Berenfeld O, Anumonwo J, Mironov SF, Udassi S, Beaumont J, Taffet S, Pertsov AM, Jalife J. Rectification of the background potassium current: a determinant of rotor dynamics in ventricular fibrillation. *Circ Res*. 2001;89:1216–1223. doi: 10.1161/hh2401.100818.

13. Samie FH, Mandapati R, Gray RA, Watanabe Y, Zuur C, Beaumont J, Jalife J. A mechanism of transition from ventricular fibrillation to tachycardia: effect of calcium channel blockade on the dynamics of rotating waves. *Circ Res*. 2000;86:684–691. doi: 10.1161/01.RES.86.6.684.

14. Berenfeld O, Zaitsev AV, Mironov SF, Pertsov AM, Jalife J. Frequency-dependent breakdown of wave propagation into fibrillatory conduction across the pectinate muscle network in the isolated sheep right atrium. *Circ Res*. 2002;90:1173–1180. doi: 10.1161/01.RES.0000022854.95998.5C.

15. Zaitsev AV, Berenfeld O, Mironov SF, Jalife J, Pertsov AM. Distribution of excitation frequencies on the epicardial and endocardial surfaces of fibrillating ventricular wall of the sheep heart. *Circ Res*. 2000;86:408–417. doi: 10.1161/01.RES.86.4.408.

16. Chen J, Mandapati R, Berenfeld O, Skanes AC, Jalife J. High-frequency periodic sources underlie ventricular fibrillation in the isolated rabbit heart. *Circ Res*. 2000;86:86–93. doi: 10.1161/01.RES.86.1.86.

17. Guillem MS, Climent AM, Millet J, Arenal Á, Fernández-Avilés F, Jalife J, Atienza F, Berenfeld O. Noninvasive localization of maximal frequency sites of atrial fibrillation by body surface potential mapping. *Circ Arrhythm Electrophysiol*. 2013;6:294–301. doi: 10.1161/CIRCEP.112.000167.

18. Massé S, Downar E, Chauhan V, Sevaptsidis E, Nanthakumar K. Ventricular fibrillation in myopathic human hearts: mechanistic insights from *in vivo* global endocardial and epicardial mapping. *Am J Physiol Heart Circ Physiol*. 2007;292:H2589–H2597. doi: 10.1152/ajpheart.01336.2006.

19. Nair K, Umapathy K, Farid T, Masse S, Mueller E, Sivanandan RV, Poku K, Rao V, Nair V, Butany J, Ideker RE, Nanthakumar K. Intramural activation during early human ventricular fibrillation. *Circ Arrhythm Electrophysiol*. 2011;4:692–703. doi: 10.1161/CIRCEP.110.961037.

20. Bradley CP, Clayton RH, Nash MP, Mourad A, Hayward M, Paterson DJ, Taggart P. Human ventricular fibrillation during global ischemia and reperfusion: paradoxical changes in activation rate and wavefront complexity. *Circ Arrhythm Electrophysiol*. 2011;4:684–691. doi: 10.1161/CIRCEP.110.961284.

21. Wit AL, Dillon SM, Coromilas J, Saltman AE, Waldecker B. Anisotropic reentry in the epicardial border zone of myocardial infarcts. *Ann N Y Acad Sci*. 1990;591:86–108.

22. Coromilas J, Costeas C, Deruyter B, Dillon SM, Peters NS, Wit AL. Effects of pinacidil on electrophysiological properties of epicardial border zone of healing canine infarcts: possible effects of K(ATP) channel activation. *Circulation*. 2002;105:2309–2317.

23. Zaitsev AV, Guha PK, Sarmast F, Kolli A, Berenfeld O, Pertsov AM, de Groot JR, Coronel R, Jalife J. Wavebreak formation during ventricular fibrillation in the isolated, regionally ischemic pig heart. *Circ Res*. 2003;92:546–553. doi: 10.1161/01.RES.0000061917.23107.F7.

24. Vaquero M, Calvo D, Jalife J. Cardiac fibrillation: from ion channels to rotors in the human heart. *Heart Rhythm*. 2008;5:872–879. doi: 10.1016/j.hrthm.2008.02.034.

25. Kim YH, Yashima M, Wu TJ, Doshi R, Chen PS, Karagueuzian HS. Mechanism of procainamide-induced prevention of spontaneous wave break during ventricular fibrillation. Insight into the maintenance of fibrillation wave fronts. *Circulation*. 1999;100:666–674. doi: 10.1161/01.CIR.100.6.666.

26. Wu TJ, Lin SF, Baher A, Qu Z, Garfinkel A, Weiss JN, Ting CT, Chen PS. Mother rotors and the mechanisms of D600-induced type 2 ventricular fibrillation. *Circulation*. 2004;110:2110–2118. doi: 10.1161/01.CIR.0000143834.51102.91.

27. Wu TJ, Ong JJ, Hwang C, Lee JJ, Fishbein MC, Czer L, Trento A, Blanche C, Kass RM, Mandel WJ, Karagueuzian HS, Chen PS. Characteristics of wave fronts during ventricular fibrillation in human hearts with dilated cardiomyopathy: role of increased fibrosis in the generation of reentry. *J Am Coll Cardiol*. 1998;32:187–196.

28. Calvo D, Atienza F, Jalife J, Martínez-Alzamora N, Bravo L, Almendral J, González-Torrecilla E, Arenal Á, Bermejo J, Fernández-Avilés F, Berenfeld O. High-rate pacing-induced atrial fibrillation effectively reveals properties of spontaneously occurring paroxysmal atrial fibrillation in humans. *Europace*. 2012;14:1560–1566. doi: 10.1093/europace/eus180.

29. Pak HN, Oh YS, Liu YB, Wu TJ, Karagueuzian HS, Lin SF, Chen PS. Catheter ablation of ventricular fibrillation in rabbit ventricles treated with beta-blockers. *Circulation*. 2003;108:3149–3156. doi: 10.1161/01.CIR.0000104563.12408.12.

30. Burnes JE, Taccardi B, Rudy Y. A noninvasive imaging modality for cardiac arrhythmias. *Circulation*. 2000;102:2152–2158. doi: 10.1161/01.CIR.102.17.2152.

31. Yokokawa M, Desjardins B, Crawford T, Good E, Morady F, Bogun F. Reasons for recurrent ventricular tachycardia after catheter ablation of post-infarction ventricular tachycardia. *J Am Coll Cardiol*. 2013;61:66–73. doi: 10.1016/j.jacc.2012.07.059.

32. Marrouche NF, Verma A, Wazni O, Schweikert R, Martin DO, Saliba W, Kilicaslan F, Cummings J, Burkhardt JD, Bhargava M, Bash D, Brachmann J, Guenther J, Hao S, Beheiry S, Rossillo A, Raviele A, Themistoclakis S, Natale A. Mode of initiation and ablation of ventricular fibrillation storms in patients with ischemic cardiomyopathy. *J Am Coll Cardiol*. 2004;43:1715–1720. doi: 10.1016/j.jacc.2004.03.004.

Circulation
Arrhythmia and Electrophysiology

Ventricular Tachycardia and Early Fibrillation in Patients With Brugada Syndrome and Ischemic Cardiomyopathy Show Predictable Frequency-Phase Properties on the Precordial ECG Consistent With the Respective Arrhythmogenic Substrate

David Calvo, Felipe Atienza, Javier Saiz, Laura Martínez, Pablo Ávila, José Rubín, Benito Herreros, Ángel Arenal, Javier García-Fernández, Ana Ferrer, Rafael Sebastián, Pablo Martínez-Camblor, José Jalife and Omer Berenfeld

The online version of this article, along with updated information and services, is located on the
World Wide Web at:
http://circep.ahajournals.org/content/8/5/1133
Free via Open Access

Data Supplement (unedited) at:
http://circep.ahajournals.org/content/suppl/2015/08/06/CIRCEP.114.002717.DC1.html

SUPPLEMENTAL MATERIAL

Supplemental Methods

Patients

Patients were admitted for electrophysiology (EP) study with either Brugada Syndrome (BrS) or Ischemic Cardiomyopathy (IC). The goal in the BrS cohort was to assess the risk profile according to the clinical standards that recommended testing for inducibility of sustained VF in patients displaying spontaneous type-I ECG pattern. The IC cohort conformed to patients with healed myocardial infarction (MI, >6 months) and sustained ventricular tachycardia (VT) that were admitted to our institutions for a catheter based ablation procedure. The study was approved by the Ethics Committee and subjects gave informed consent.

Electrophysiology and Recording Protocol

EP Study was performed in the fasting, unsedated state. All antiarrhythmic drugs were discontinued prior to study. In all patients x12 lead standard ECG was recorded continuously at 1 KHz sampling rate and 0.05-150 Hz band-pass filtering. The EP strategy varied according to the clinical indication as follows:

i) Brugada syndrome patients: programmed stimulation was used to induce VF. A tetrapolar catheter was positioned in the right ventricular apex (RVA). A second catheter at the right ventricular outflow tract (RVOT) was considered optional. Programed ventricular stimulation at the RVA was performed using trains of pulses with a basic cycle length of 600/400 ms, and up to 3 extra stimuli limited by tissue refractoriness or maximum coupling interval of 200 ms. If RVA stimulation failed to induce sustained VF, the protocol was repeated pacing from the RVOT. Patients were included in the study only if the immediately preceding ECG displayed a type-I ECG pattern on the right precordial leads (V1 and V2).

ii) Ischemic cardiomyopathy patients: programmed stimulation was used to induce VT (VF induction was unintentional by protocol). A tetrapolar catheter was placed in the RVA and a 3.5 mm irrigated tip catheter (Navistar Thermocool®, Biosense Webster) was placed in the left ventricle (LV) for endocardial mapping and ablation. The VT

ablation procedure included the following: 3D endocardial reconstructions were created by CARTO (Biosense Webster) delineating endocardial scar tissue as areas displaying bipolar electrogram amplitudes of <1.5 mV and dense scar tissue with electrogram amplitudes of <0.5 mV. Ablation followed mapping of induced and/or spontaneous sustained VT. Careful attention was paid to localize the exit site of the VT in relation to the myocardial scar. Areas displaying presystolic electrograms (within 50 ms before the QRS onset) and fulfilling the criteria of concealed entrainment with equally spike-QRS to electrogram-QRS intervals were considered at the tachycardia exit site and annotated in the 3D maps. When no sustained VT was inducible, or fast VT induction required cardioversion, a substrate-based ablation was performed consisting of RF ablation and elimination of delayed electrograms in the scar areas as described.[1] The IC patients included in the study were those in whom sustained VF was unintentionally induced, either by pacing or while moving the catheters. In a subset of 6 patients, CT-Scan images were merged with the CARTO mapping for better anatomical reference. The positions of the precordial ECG leads at the thorax surface were marked by acquiring the corresponding location of catheter tip points on the CARTO. Continuous pacing from the RVOT and RVA was performed to allow for controlled origin of propagated waves and validation of methods.

Processing of Precordial ECG Signals

ECG signals from precordial V1-V6 leads (Figure S2) were exported for off-line analysis. VF and VT were classified based on the morphology of the surface recordings and the regularity of bipolar signals from the right and left ventricular endocardium. Precordial signals were processed by a Hanning window and with a non-biased 1-20 Hz band-pass filter to minimize baseline wander and high-frequency harmonics (Sigview® v2.3, SignalLab). Thereafter, a 4096-point fast Fourier transformation (FFT, spectral resolution 0.24 Hz) was obtained for frequency and phase analysis. Power and phase versus frequency were calculated for sliding episodes with 15 ms leaps (periodograms). Dominant frequency (DF) was defined as the frequency of highest power in the power spectrum. Power spectra obtained by FFT for the 6 precordial leads were also analyzed for spatiotemporal patterns across time. A shared frequency (SF) was defined as a frequency with power peak lasting more than 0.5 sec concurrently in all leads (Figure 1). The life-span of the SF was quantified as the time interval between

its appearance and disappearance as a discrete power peak in the periodogram of all precordial leads. Phase was calculated by two methods, as follows: (i) the instantaneous phase at the SF was calculated based on the ratio of the imaginary to the real components of the FFT at the SF frequency of the sliding episodes; (ii) the instantaneous phase of the activity, considering its entire frequency spectrum, was calculated based on its Hilbert transform.[2] The calculated phases were plotted against the time of the sliding episodes for all the precordial leads (Figure 2 and Figure S2). The time-course of the phases in each precordial lead enabled the analysis of their relative timing and sequence of activation. The phase time-courses of the leads during VF and VT were found to cluster in groups separated by periodic intervals that were >50% longer than the 2nd ranked intervals (Figure 2). Two characteristics of the phase clusters were quantified: first, for the instantaneous distribution of the level of activity across leads, we determined the phase distribution at a particular time as early (top) to late (bottom, Figure 2 panel A; black arrow); Second, for the propagation of the activity across leads we determined progression of time for a fixed phase (Phase propagation; Figure 2, panel A; red arrow).

Computer Simulations

Simulated body surface potentials during ventricular pacing were computed for validation in a 3D realistic model of human heart and torso. The ventricular model[3] was segmented from a human diffusion tensor magnetic resonance imaging (DTMRI) dataset with hexahedral elements 0.5 mm size (1.43 million nodes). ten Tusscher et al membrane kinetics[4] were used to simulate heterogeneous action potentials and excitation propagation using an operator splitting method with adaptive time step (>0.02 ms). The human torso was segmented from magnetic resonance data considering bone, muscle, blood, lung and liver properties. The inhomogeneous torso consisted of 134,600 nodes and 755,394 tetrahedrons, with a mean distance of 0.6 cm between nodes.[5]
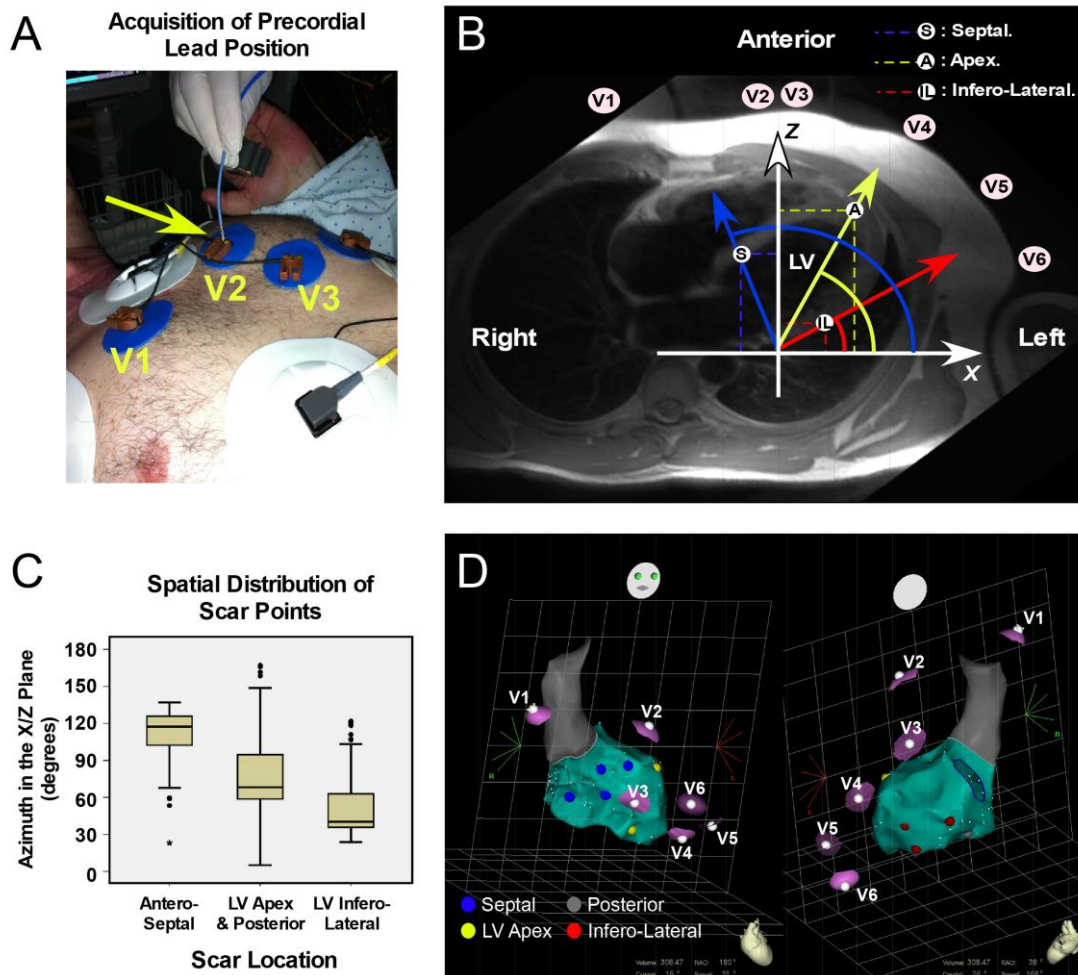
Statistical Analysis

Continuous variables are reported as mean±standard deviation (SD) or followed by 95% Confidence Interval (CI95%). Categorical variables are reported as number and

percentage. In the case of nondependent variables we used the Chi-Square test (categorical variables) and unpaired or pairwise t-test (continuous variables) for comparisons as appropriate. Pearson's coefficient is also used to compute linear correlation in the case of nondependent data. Kernel density estimator is used to estimate de density function of data distribution when appropriate.[6] The estimation is computed directly using the R "density" function (R version 3.1 [www.r-project.org]) and the used kernel is Gaussian.

Resampling methods have been used to make inferences when dealing with complex data structures; e.g., where different observations could be drawn from the same subject (dependency structures). Specifically, the naive bootstrap[7] and the general bootstrap algorithm (gBA)[8] were used for confidence intervals and testing, respectively. In both cases, the resampling was made on the subjects. In this context, correlation coefficients were calculated based on general additive models and taking into account the dependent data structure. The concordance correlation coefficient (k coefficient) was computed when appropriate with CI95%: also computed by resampling methods. Analyses were performed with R version 3.1 (www.r-project.org), Origin 8.1 (OriginLab Corp, Northampton, MA) and Matlab R2014a (Mathworks, Natick, MA). Statistical significance was established at $p<0.05$.
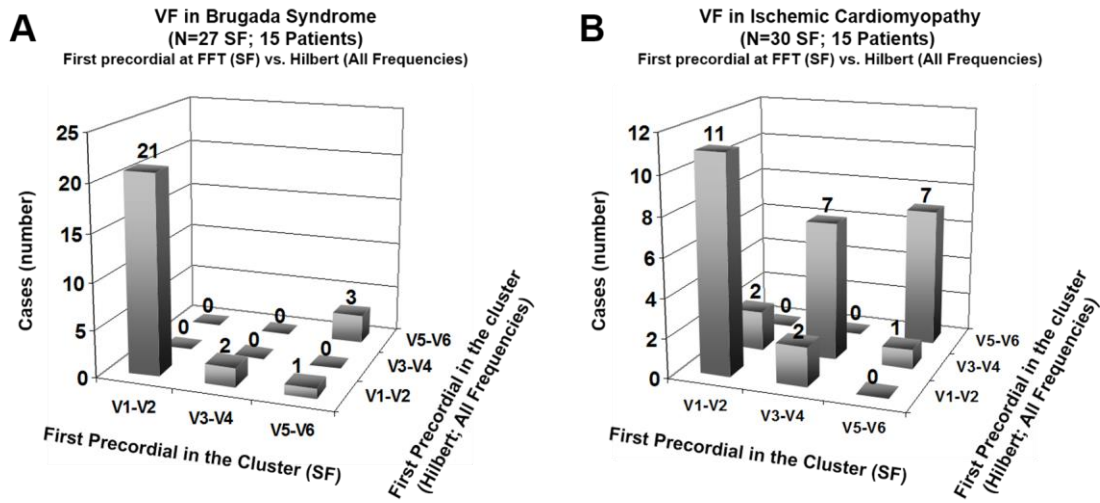
Figure S1

Localization of the precordial leads, scar tissue and exit sites using the Electro-anatomical mapping system. **A.** Acquisition of the precordial leads spatial location. The yellow arrow points to the tip of the CARTO catheter in contact with the precordial lead V2 to acquire its location for display in 3D maps as shown in Panel D. **B.** Illustration of the quantification of the scar tissue location on a short-axis of magnetic resonance image of the thorax. The X-Z coordinates of the scar points (bipolar < 0.5 mV) were exported from the 3D navigation system for every patient. A cross-patient invariable origin of the coordinate system was localized to 0.35 distance units to the left of the most right aspect of the LV (X=0) and the most posterior aspect of the LV (Z=0) for each patient (a location corresponding to the mid-basal aspect of the LV). The angle of each scar point (azimuth) was then calculated as arctan(Z/X), independently from
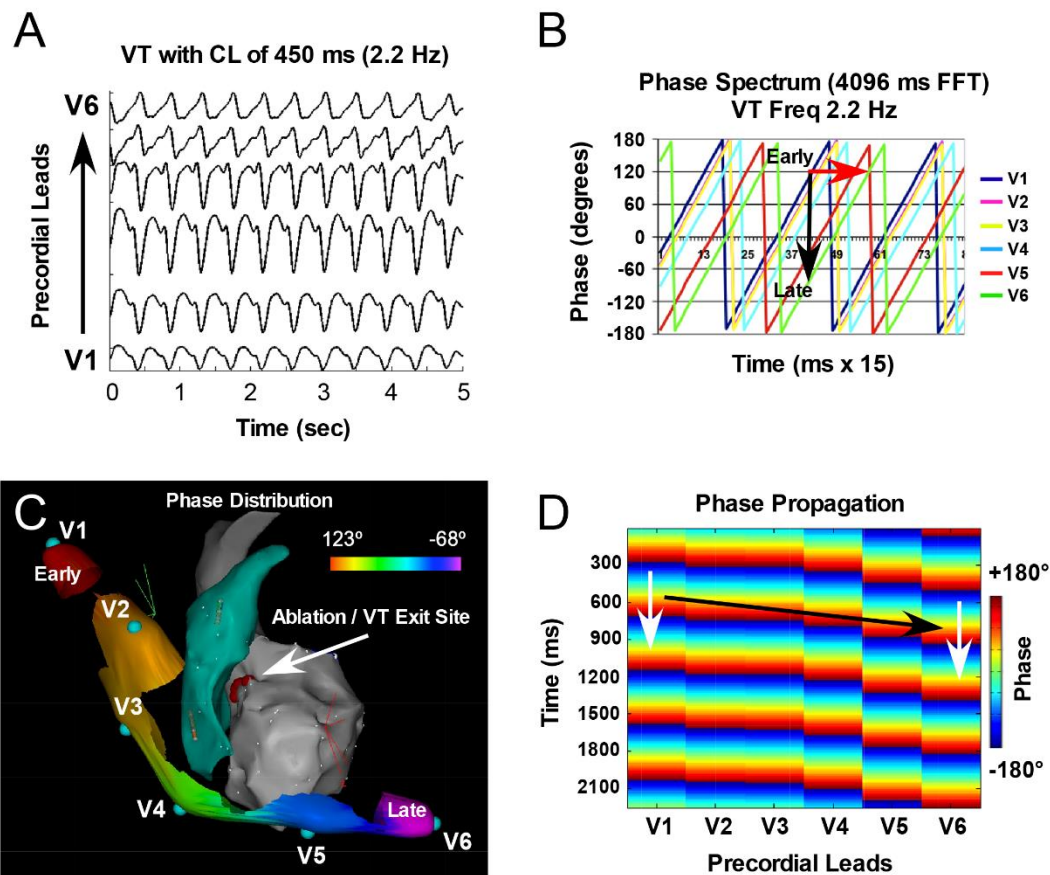
the heart size of each patient. For illustration, 3 sample points at Septum, LV Apex and LV Infero-Lateral wall were marked with their distance vectors in the common coordinate system denote an increase in the angle displayed as they change in position from the lateral to the apex and the septal aspects of the LV. In addition, the projection of the 6 precordial leads on the same (X,Z) plane was used for the calculation of the angle of the leads (Panel D). **C.** The (X,Z) plane azimuth for 362 scars points classified each one prior to the angle calculation as being part of antero-septal, apex-posterior or infero-lateral scars in a subset of 6 patients for whom the position of the precordials were also recorded from the 3D navigation system. Box-plots depict the median, 25 and 75 percentile. Dots outside the boxes are the outliers and bars represents the "inner fences", which extend to 1.5 times the height of the box. The figure shows that despite physiological overlap between the 3 scar locations, their (X,Z) plane azimuths are distinguishable. Due to the complexity of the data structure and the sparse sample size available, in this analysis we only describe the results and refrain from a hypothesis testing and quantified probabilities (p-values) which do not provide additional information. **D.** The VT exit sites in 10 patients are superimposed on a reference individual endocardial map displaying also the precordial leads position. The incorporation of exits sites on a common map was used for the calculation of the exits sites and precordial azimuths in the same coordinates system.
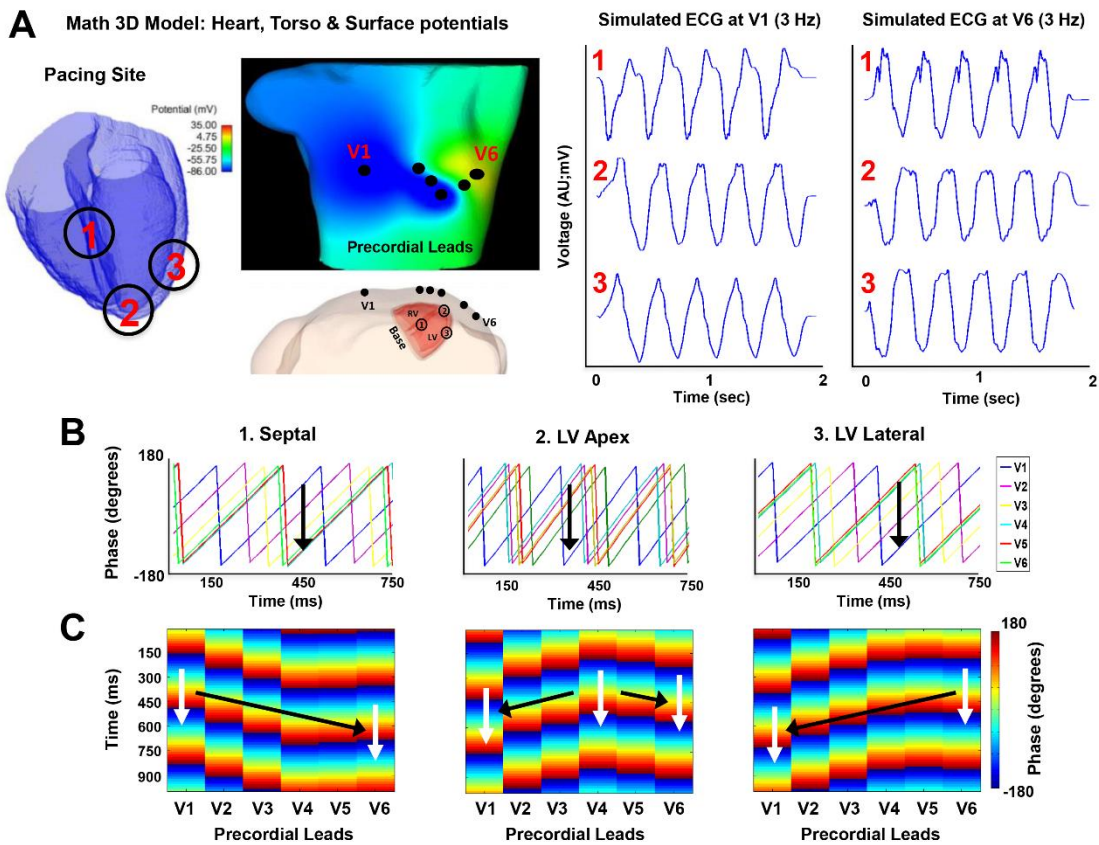
Figure S2

Concordance between the precordial leads origin obtained thorough FFT- and Hilbert-based phase propagation analysis during VF. The concordance correlation coefficient (*k* coefficient) observed between both methods (FFT vs. Hilbert Phase) was 0.741 (CI95%: 0.497-0.938; computed by resampling methods). **A.** Distribution of data in BrSugada Syndrome patients. **B.** Distribution of data in Ischemic Cardiomyopathy patients.
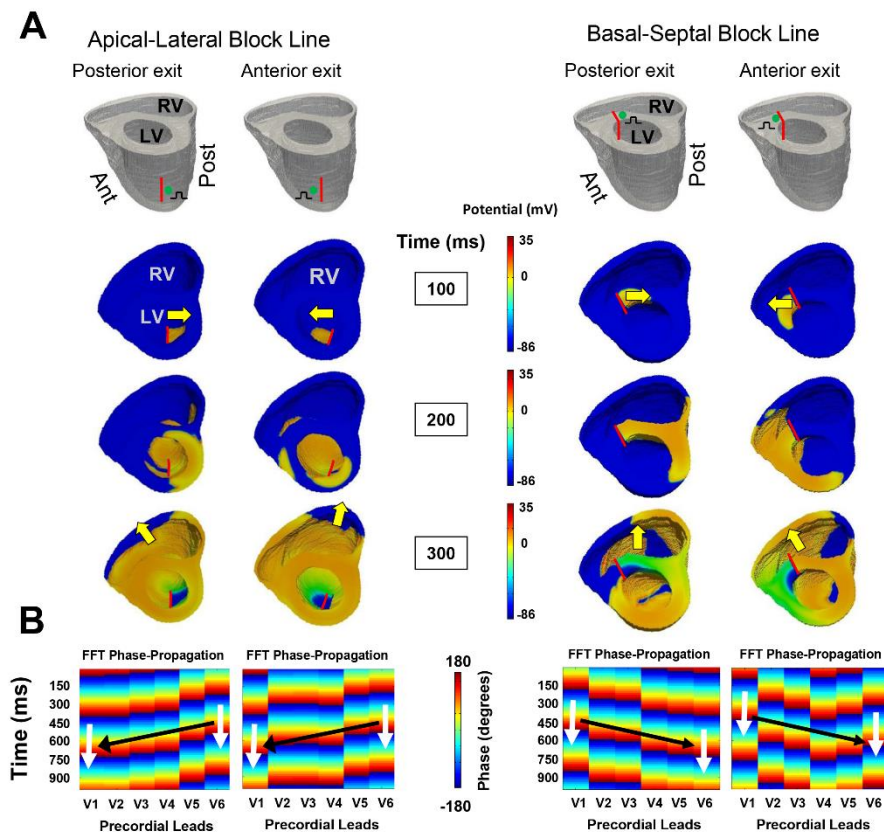
Figure S3

A representative example of the phase approach applied to a monomorphic VT. **A.** Precordial ECG tracings of the mapped VT. **B.** Time course of FFT-based phase at 2.2 Hz (the VT frequency). Black arrow denotes the sequence of phases from V1 to V6 at a fixed time. Red arrow indicates phase propagation across leads and time. **C.** 3D map displaying the RV, LV and superimposed color-coded phase distribution map in the precordial leads (timed at the black arrow in panel B). The VT exit site is marked with red dots at the high and basal LV septum. **D.** Phase propagation diagram denotes time-independent activation sequence from V1 to V6. Overall, the phase distribution and propagation is in agreement with what is expected from the exit site of the VT as illustrated in Panel C and D.
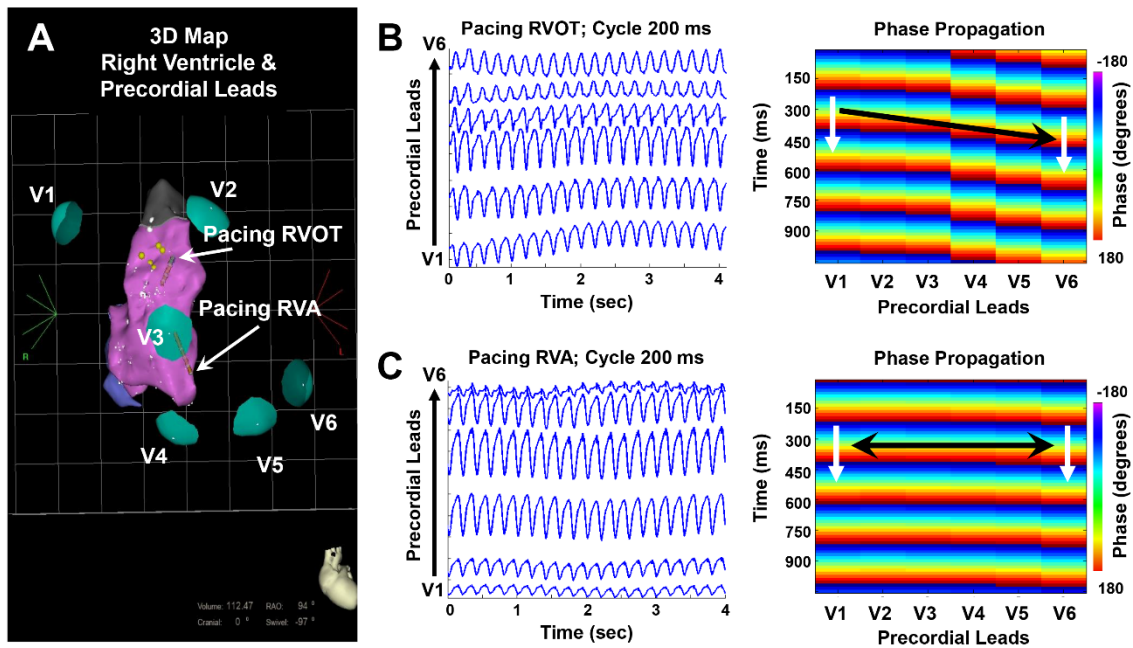
Figure S4

Validation of the phase analysis using computer simulations. **A.** A realistic computer model of human ventricles and torso was used to simulate ventricular wave propagation and precordial lead ECGs during pacing. The right side traces show simulated ECG signals at the indicated pacing and recording sites. **B.** Pacing from septal (1), apex (2) and lateral (3) ventricular sites resulted in varying sequences of phase distribution across the precordial leads. Black arrows depict the distribution of phases from early to late at a sample instant. **C.** Plots of phase/time (white arrows) vs. lead number (black arrows) show phase propagation. The direction of propagation of FFT phases during pacing shows dependency on the directionality of wavefront propagation. Septal pacing (left) results in a V1 to V5-V6 propagation; LV lateral pacing (right) reverses propagation from V5-V6 to V1. LV apex pacing (middle) results in propagation toward V1 and V6. AU: arbitrary units.
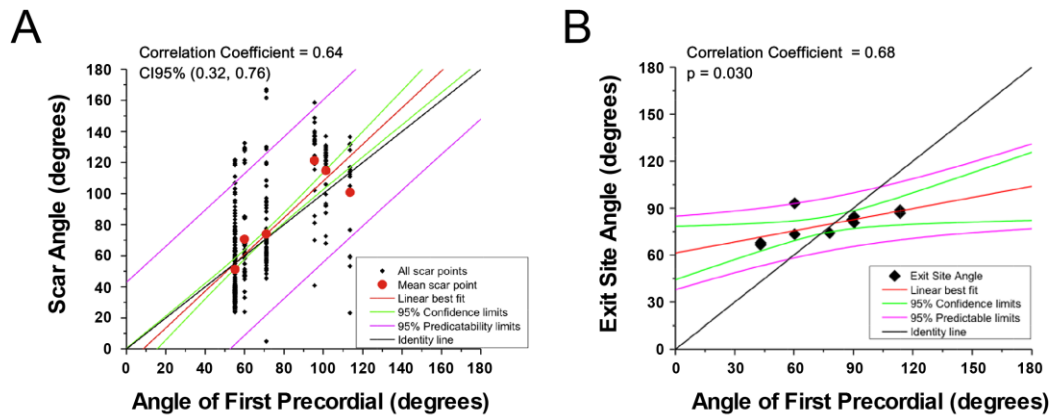
Figure S5

Phase analysis for waves originating at the same scar, but propagating in opposite directions (opposite exit sites). **A.** Top, views of the ventricles with conduction block lines (red lines) modeling scars of typical sizes in the septum and lateral aspects of the LV. Pacing is on either side of the block line (green dots) to simulate waves originating at those scars, but moving in opposite directions. Bottom, basal view of the models with color-coded transmembrane potential for the four pacing sites. Tracking the wave propagation for each block line reveals that following a brief period in which waves moved in opposite directions (yellow arrows at 100 ms), the subsequent pattern of wave of propagation ended up being similar irrespective of the initial exit site (yellow arrows at 300 ms). **B.** Plots of phase/time (white arrows) vs. lead number (black arrows) reproduce the sequences observed in IC patients (Figures 3 and 4) and show that although phase propagation maps are somewhat sensitive to the particular direction of the waves at their exit sites, the general pattern of propagation is more strongly affected by the spatial location of the wave origin (V6 to V1 when the exit sites are on the lateral wall; V1 to V6 first when the exit sites are on the septum).

Figure S6

Phase propagation of paced waves from two different locations in the right ventricle. **A.** 3D map of the right ventricle with the pacing sites at the apex (RVA) and the outflow tract (RVOT). **B.** Precordial ECG signals during high frequency pacing (cycle length 200 ms) at the RVOT and the corresponding phase propagation diagrams. **C.** Precordial ECG signals during the same pacing frequency (cycle length 200 ms) at the RVA and the corresponding phase propagation diagrams. Despite limitations in the time domain analysis of the ECG tracings at high frequency, phase propagation sequence remains sensitive to the spatial location of the pacing site and to the myocardial patterns of propagation.

Figure S7

Correlations between the (*X,Z*) plane angles (azimuths; see Figure S1) of the scar and VT exit site locations with the angle of the first precordial to be activated during VF and VT respectively. **A.** Correlation observed between the azimuth of 362 scar points in 6 different patients and the azimuth of the first precordial being activated during VF (data from patients included in panel C of Figure S1). The Identity line (black) is very close to the linear best fit line (red line) and the identity line also falls well inside the 95% predictability line (magenta). Both facts corroborate the notion that the first precordial lead in the phase analysis can be used to guide for the location of the scar. Due to the complexity of the data structure and the sparse sample size available (N=6), in this analysis we report only 95% confidence intervals computed by resampling methods (omitting p-values). **B.** The azimuth in the (*X,Z*) plane for each VT exit site was correlated with the azimuth of the first precordial that is being activated at each cycle during VT. (Not to be confused with exit sites generating opposing wave propagation as simulated in Fig. S4) A significant correlation was observed, which enhances the significance of the phase-propagation patterns as dependent on the origin of the electrical propagation in the myocardium.

Supplemental References

1. Arenal A, del Castillo S, Gonzalez-Torrecilla E, Atienza F, Ortiz M, Jimenez J, Puchol A, García J, Almendral J. Tachycardia-related channel in the scar tissue in patients with sustained monomorphic ventricular tachycardias: influence of the voltage scar definition. *Circulation*. 2004; 110:2568–2574.

2. Warren M, Guha PK, Berenfeld O, Zaitsev A, Anumonwo JMB, Dhamoon AS, Bagwe S, Taffet SM, Jalife J. Blockade of the inward rectifying potassium current terminates ventricular fibrillation in the guinea pig heart. *J. Cardiovasc. Electrophysiol*. 2003; 14:621–631.

3. Dux-Santoy L, Sebastian R, Felix-Rodriguez J, Ferrero JM, Saiz J. Interaction of Specialized Cardiac Conduction System With Antiarrhythmic Drugs: A Simulation Study. IEEE Trans. Biomed. Eng., 58(12): 3475-3478, 2011.

4. ten Tusscher KH, Noble D, Noble PJ, Panfilov AV. A model for human ventricular tissue. Am J Physiol Heart Circ Physiol 2004; 286:H1573-H1589.

5. Ferrer A, Sebastian R, Felix-Rodriguez J, Tobón C, Saiz J. Modeling of human torso for the study and characterization of atrial arrhythmias. Cardiac Physiome Workshop, San Diego, USA, 2012.

6. Martínez-Camblor P, de Uña-Álvarez J. Non-parametric k-sample tests: Density functions vs distribution functions. Computational Statistics and Data Analysis. 2009;53:3344–3357.

7. Efron B TR. An Introduction to the Bootstrap. New-York: Chapman & Hall; 1993.

8. Martínez-Camblor P, Corral N. A general bootstrap algorithm for hypothesis testing. Journal of Statistical Planning and Inference. 2012;142:589–600.